

Entanglement of bosons in optical lattices

M. Cramer,^{1,2} A. Bernard,³ N. Fabbri,³ L. Fallani,^{3,4} C. Fort,³ S. Rosi,³ F. Caruso,^{3,4} M. Inguscio,^{3,4} and M.B. Plenio^{1,2}

¹*Institut für Theoretische Physik, Albert-Einstein Allee 11, Universität Ulm, D-89069 Ulm, Germany*

²*Center for Integrated Quantum Science and Technology,*

Albert-Einstein Allee 11, Universität Ulm, D-89069 Ulm, Germany

³*LENS, Dipartimento di Fisica e Astronomia, Università di Firenze and INO-CNR, via Nello Carrara 1, I-50019 Sesto Fiorentino (FI), Italy, and*

⁴*QSTAR Center for Quantum Science and Technology, Largo Enrico Fermi 2, I-50125 Arcetri, Italy.*

Entanglement is a fundamental resource for quantum information processing [1, 2] which occurs naturally in many-body systems at low temperatures. The presence of entanglement and, in particular, its scaling with the size of system partitions [3–5] underlies the complexity of quantum many-body states [5–7]. The quantitative estimation of entanglement in many-body systems represents a major challenge as it is held to require either full state tomography [8], which scales exponentially in the system size, or the assumption of unverified system characteristics such as its Hamiltonian or its temperature. We adopt recently developed approaches for the determination of rigorous lower entanglement bounds from readily accessible measurements [9, 10] and apply them in an experiment of ultracold interacting bosons in optical lattices of approximately 10^5 lattice sites. We use this approach to study the behaviour of spatial entanglement between the sites when crossing the superfluid to Mott insulator transition and when varying the temperature. This constitutes the first rigorous experimental large-scale entanglement quantification in a scalable quantum simulator.

Background – The last few years have seen experiments towards the verification of the presence of entanglement in a variety of physical realizations of many-body systems. Multi-particle spin entanglement of distinguishable particles has been created and studied experimentally for up to 14 sites in ion traps [11–13] and up to eight sites in photonic setups [14] by means of entanglement witnesses that determine the presence of entanglement. In ultracold neutral atomic gases, entanglement between indistinguishable particles with two internal degrees of freedom was generated by squeezing of the total (pseudo) spin and its presence verified by spin-squeezing inequalities [15–18]. For ultra-cold bosons with two internal degrees of freedom in optical lattices, entanglement between lattice sites was created by controlled collisions and qualitative evidence for its presence was found [19]. Experimental evidence for the entanglement between the spins in magnetic materials was given by comparison of the neutron scattering structure factor to a classical description [20].

A key challenge that remains to be addressed however concerns the *quantitative* determination of upper and lower bounds on the entanglement that is present in the system *without* resorting to assumptions concerning unverified system characteristics such as its Hamiltonian or its temperature. This can be achieved by adopting a simple but powerful principle [9, 21–23] in combination with methods from optimization theory: Given a set of observables, we consider all density matrices that are compatible with experimentally measured expectation values of these observables. Amongst these density matrices, we find the one with the *least* (*largest*) amount of entanglement as quantified by a suitable entanglement measure [1]. In this way we determine a lower (upper) bound on the entanglement that must have been present in the state that gave rise to the observed expectation values. These bounds do not require any other assumptions on the system.

Fundamentals – The multi-partite entanglement that we observe and quantify in our experiment arises in a periodic optical potential (optical lattice) that hosts massive bosonic par-

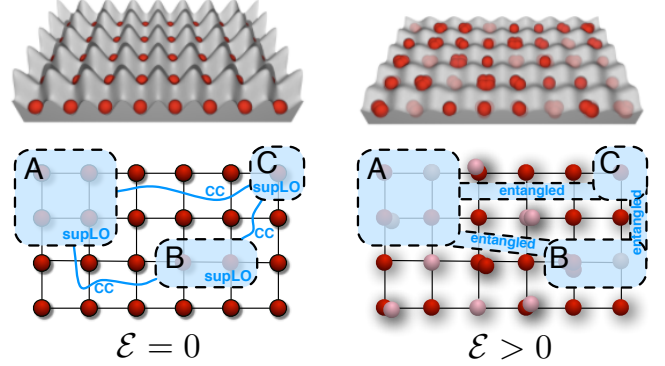


FIG. 1: We investigate entanglement in an optical lattice filled by ultracold bosons. At large lattice height, the ground state is a pure product state and no quantum correlations exist between any subset of sites (A, B, C, ...). Such a state can be created by only performing physical local operations (those that respect the mass superselection rule locally, supLO operations) and allowing the parties associated with the subsets to communicate classically (CC). Decreasing the lattice depth, the resulting state may not be created by such operations anymore – the state becomes a resource of value \mathcal{E} with which the parties may overcome their locality restrictions, i.e., entanglement is created.

ticles (see Fig. 1). Hence, the non-local correlations are unavoidably intertwined with the superselection rules that prohibit the formation of coherent superpositions with different particle numbers. As a consequence, before we can provide a *rigorous* theoretical and experimental *quantification* of the entanglement in the system, we need to clarify its nature. We achieve this from the viewpoint of entanglement as a resource [1].

Physical constraints, fundamental or practical, impose limitations on accessible physical operations [24, 25]. For example, the locality constraint that expresses the inability to ex-

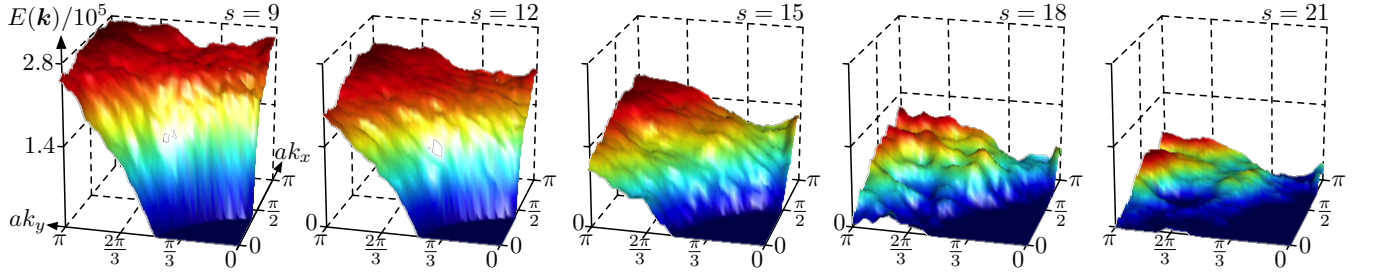


FIG. 2: The minimal entanglement $E(\mathbf{k})$ consistent with the measured momentum distributions of an atomic gas in a three-dimensional optical lattice tuned across the quantum phase transition from superfluid to Mott insulator (lattice depth $s = 9, 12, 15, 18, 21$). For each value of the momentum \mathbf{k} in the first Brillouin zone, $E(\mathbf{k})$ provides a lower bound to the entanglement present in the bosonic sample. The total number of particles was approximately 3.5×10^5 for each measurement. See Fig. 2 for total particle numbers.

change quantum particles between distant laboratories A and B prevents the execution of quantum gates between A and B . Such constraints in turn imply the existence of resources—here entangled states—that, when consumed, allow for the realization of operations that are impossible under the given physical constraints [26]. The use of entanglement in teleportation for example allows for the realization of general quantum gates between A and B [27, 28]. This aspect captures the multi-partite nature and non-local correlations in the system.

For massive bosonic particles an even more fundamental constraint concerns superselection rules for massive indistinguishable particles: Physical operations cannot create coherent superpositions of different particle numbers. In connection with the locality constraint this requires that all physically allowed local operations must commute with the local particle number operator.

The fact that both constraints, locality and super-selection rules, need to be considered *simultaneously* for massive bosonic particles leads to a refined picture of non-local resources and thus entanglement [29–32]. In a multi-partite system, as in Fig. 1, in which two or more parties aim to exchange quantum information, but are restricted (i) to only act locally on their respective quantum system and communicate classically (LOCC), and (ii) to perform only operations preserving the local particle number operator, they may (in the two-partite case) only prepare states $\hat{\rho}$ of the form

$$\hat{\rho} = \sum_n p_n \hat{\rho}_A^{(n)} \otimes \hat{\rho}_B^{(n)}, \quad (1)$$

where $\hat{\rho}_A^{(n)}$ ($\hat{\rho}_B^{(n)}$) are density operators of subsystem A (B), $\{p_n\}$ is a probability distribution and the local states must commute with the local particle number operators \hat{N}_A and \hat{N}_B , respectively, i.e., $[\hat{\rho}_A^{(n)}, \hat{N}_A] = [\hat{\rho}_B^{(n)}, \hat{N}_B] = 0$. All such states are here collected in the set \mathcal{S} . All other states, so states not in \mathcal{S} , become a resource, to be used to overcome the constraint imposed by locality and/or superselection rules (see Appendix A for an illustrative example).

Entanglement Quantification: Theory – Having clarified these fundamental issues, the key point is now that we turn this *qualitative* appreciation of the value of these states into a mathematically and physically well defined *quantifier* that

may then be determined experimentally. It is a crucial requirement that the value of this quantifier does not increase on average under LOCC operations that respect local superselection rules (supLOCC in short). Such a quantifier is then denoted a supLOCC monotone. To this end, we define \mathcal{W} as the set of entanglement witnesses \hat{W} [33] satisfying (i) $\text{tr}[\hat{W}\hat{\rho}] \geq 0$ for all $\hat{\rho} \in \mathcal{S}$ and (ii) the operator inequality $\hat{W} + \hat{N} \geq 0$. Then

$$\mathcal{E}(\hat{\rho}) = \max\left\{0, -\inf_{\hat{W} \in \mathcal{W}} \text{tr}[\hat{W}\hat{\rho}]\right\} \quad (2)$$

is a supLOCC monotone (see Appendix B for a proof and note the similarity to entanglement monotones expressed as optimization over witnesses for spin systems in Ref. [34]). Note that, for any state $\hat{\rho}$, its entanglement $\mathcal{E}(\hat{\rho})$ is upper bounded by the mean total number of particles $\langle \hat{N} \rangle = \text{tr}[\hat{N}\hat{\rho}]$, providing a figure of merit for the lower bounds we will present below. This definition may be straightforwardly extended to more than two parties and we now set out to quantify the entanglement under superselection rules contained in states of bosons in optical lattices when each lattice site constitutes a party, i.e., labelling the sites of the three-dimensional lattice by $\mathbf{i} = (i_1, i_2, i_3)$, states in \mathcal{S} are of the form $\sum_n p_n \bigotimes_{\mathbf{i}} \hat{\rho}_{\mathbf{i}}^{(n)}$ with $[\hat{\rho}_{\mathbf{i}}^{(n)}, \hat{n}_{\mathbf{i}}] = 0$, where $\hat{n}_{\mathbf{i}}$ is the number operator for the lattice site \mathbf{i} . In this way, we quantify the entanglement shared between *sites* of the lattice (as opposed to between particles).

Needless to say, Eq. (2) is exceedingly hard to compute analytically or even numerically, especially in the many-particle system (where each constituent is in addition being described in an infinite-dimensional Hilbert space) that we consider here. However, rather than aiming for exact values we will follow Refs. [9, 21, 22, 32] to derive lower bounds to Eq. (2) which, after the introduction of essential aspects of the experimental setup, we will demonstrate to be obtained from readily accessible measurements.

Experiment – In the experiment we quantify the entanglement of a system of ultracold interacting bosons in a three dimensional lattice potential. An almost pure [35] Bose-Einstein condensate of $\approx 3.5 \times 10^5$ atoms of ^{87}Rb is prepared evaporating a sample of atoms in the $|F = 1, M_F = -1\rangle$ state in a hybrid trap composed of a focused red detuned laser beam (optical dipole trap ODT) propagating in the horizontal

plane plus a quadrupole magnetic field. As first demonstrated in [36], when the focused laser beam is slightly offset vertically from the center of the quadrupole magnetic field, the atoms experience a harmonic potential with cylindrical symmetry. In our system the resulting frequencies are ≈ 50 Hz and ≈ 8 Hz in the radial and axial directions respectively. An optical lattice (OL) potential with lattice constant $a = \lambda/2$, generated by three counter-propagating red-detuned beams (with wavelength $\lambda = 830.3$ nm and waists $w \approx 180$ μ m) is slowly superimposed to the sample by performing an exponential ramp in $t_{\text{ramp}} = 140$ ms. The final amplitude of the lattices $V_{\text{OL}} = sE_{\text{R}}$ (where $E_{\text{R}} = \hbar^2/(2m\lambda^2)$ is the recoil energy associated to the absorption of a lattice photon by an atom with mass m) has been calibrated with an accuracy of $\pm 10\%$ through lattice amplitude modulation spectroscopy [37] and can be varied from $s = 0$ to $s = 30$. In this way, we realize a many-body state of bosons in a three dimensional cubic lattice (subject to the harmonic trapping potential), the entanglement of which we are interested in quantifying. The system's Hamiltonian is well approximated by the Bose-Hubbard Hamiltonian [38] (note that this information/approximation will not enter into our quantification of the entanglement). At sufficiently low temperatures, when the lattice depth is $s \gtrsim 15$, the ratio between the interaction energy U of two atoms in the same lattice site and the tunnel energy J between two adjacent lattice sites is large enough to obtain a Mott insulator as firstly demonstrated in [39]. Due to the overall harmonic confinement an inhomogeneous Mott insulator is obtained with regions with different filling. At $s = 27$, we estimate $\sim 70\%$ of the atoms (in the outer region of the sample) to be in a Mott shell with 1 atom per site and $\sim 30\%$ (in the central region) to be in a Mott shell with 2 atoms per site.

We now describe the experimental procedure—time-of-flight measurements—which will give access to an observable allowing us to lower bound the entanglement of the bosons in the optical lattice. After a holding time $t_{\text{hold}} = 5$ ms, we simultaneously switch off both the trap and the optical lattice. The cloud then expands freely for a time $t_{\text{tof}} = 21$ ms before we measure the column density through absorption imaging. In practice, we measure the optical density $\mu(x, y)$ of the atomic sample integrated along the direction of the imaging laser beam, and we extract the real atomic (column) density

$$n(x, y) = \alpha (\mu(x, y) - \mu_0) \quad (3)$$

with α being a pre-factor related to the imaging calibration and the effective size of the CCD square pixel, as discussed in Appendix D, and μ_0 is the background noise level of the image, that is mainly due to residual fluctuations in the laser intensity of the imaging beam.

Entanglement Quantification: Experiment – From the column density $n(x, y)$ we can extract a lower bound to the entanglement \mathcal{E} as follows. The column density at position $(x, y) = \mathbf{r} = \hbar t \mathbf{k}/m$ (where $\mathbf{k} = (k_x, k_y)$ is the quasi-momentum in the lattice) after a time of flight t is given by

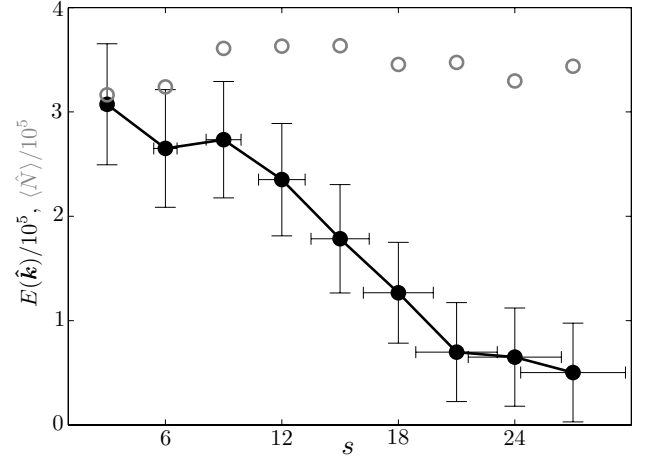


FIG. 3: Minimal entanglement $E(\hat{\mathbf{k}})$ consistent with time-of-flight measurements as a function of the lattice depth s . The reported data correspond to the average of the lower bound $E(\mathbf{k})$ over 5×5 pixels centered at $\hat{\mathbf{k}} = (\pi/a, \pi/a)$. Lines are guides to the eye. Error bars include statistical and systematic errors due to the uncertainty in the lattice depth and in the image acquisition and processing, see Appendix D for details. Circles in grey show the corresponding mean total number of bosons (without error bars for clarity, relative error $\approx 8\%$) which upper bounds the entanglement as discussed in the text after Eq. (2).

[40, 41]

$$\hat{n}(\mathbf{k}) = f(\mathbf{k}) \sum_{\substack{i,j \\ i_z=j_z}} \hat{b}_i^\dagger \hat{b}_j e^{i\mathbf{k} \cdot (\mathbf{i}-\mathbf{j})} e^{i\frac{ma^2}{2\hbar t}(\mathbf{j}^2 - \mathbf{i}^2)}, \quad (4)$$

where \hat{b}_i^\dagger (\hat{b}_i) is the creation (annihilation) operator of a particle at the lattice site i and $f(\mathbf{k}) > 0$ may be obtained from a numerical band-structure calculation (See Appendix C for details).

It is straightforward to show [9] that $\hat{W}(\mathbf{k}) := \hat{n}(\mathbf{k})/f(\mathbf{k}) - \hat{N} \in \mathcal{W}$, where \hat{N} is the total particle number operator, so that it is a witness as required in Eq. (2). Then, for any state $\hat{\rho}$, we have a lower bound to its entanglement content in terms of $\langle \hat{N} \rangle = \text{tr}[\hat{\rho}\hat{N}]$ and $\langle \hat{n}(\mathbf{k}) \rangle = \text{tr}[\hat{\rho}\hat{n}(\mathbf{k})]$:

$$\mathcal{E}(\hat{\rho}) \geq \max\left\{0, \langle \hat{N} \rangle - \frac{\langle \hat{n}(\mathbf{k}) \rangle}{f(\mathbf{k})}\right\} =: E(\mathbf{k}), \quad (5)$$

which holds for all \mathbf{k} . Note that there are no assumptions: The entanglement of any state is bounded from below by Eq. (5). The Hamiltonian governing the system, the temperature, details of external potentials, or even the system being in equilibrium, need not to be assumed.

As $E(\mathbf{k})$ is a lower bound to the entanglement $\mathcal{E}(\hat{\rho})$ for all \mathbf{k} , averages over an area A , $\int_A d\mathbf{k} E(\mathbf{k})/|A|$, also provide lower bounds. We use this fact to account for the finite resolution of the camera and to incorporate symmetries (see Appendix D details). For ease of notation, we denote this lower bound also by $E(\mathbf{k})$.

We determine the minimal entanglement $E(\mathbf{k})$ for different optical lattice depths across the superfluid to Mott insulator

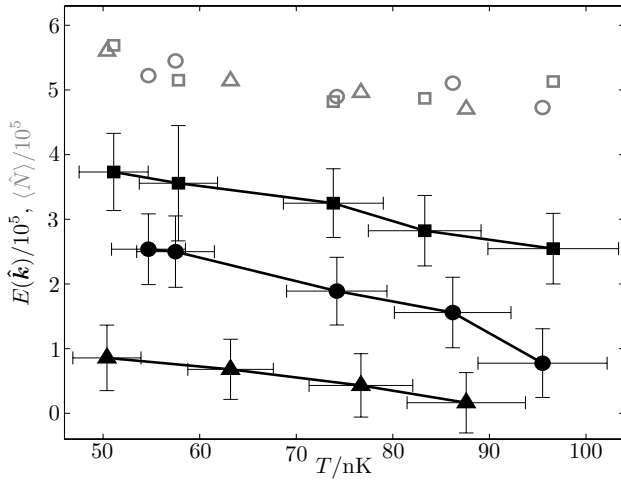


FIG. 4: Lower bound $E(\hat{\mathbf{k}})$ as a function of temperature for three different values of the lattice depth [$s = 6$ (filled boxes), $s = 12$ (filled circles), $s = 18$ (filled triangles)] following the caption of Fig. 3. Corresponding non-filled symbols in grey show the mean total number of bosons. Horizontal error bars indicate the uncertainty due to the calibration of the imaging system (error bars on mean total number of atoms not shown for clarity, relative error was $\approx 8\%$).

transition. Before presenting our experimental results, let us consider the two extreme cases analytically. For ultra-deep lattices ($s \rightarrow \infty$) and at zero temperature, the system will be in a Fock state $|n_1 n_2 \dots\rangle$, for which $\mathcal{E} = E(\mathbf{k}) = 0$ by definition. For very shallow lattices, when tunnelling dominates over the on-site repulsion and one neglects the latter, the ground state with N particles of the translationally invariant Bose-Hubbard Hamiltonian is proportional to $(\sum_i \hat{b}_i^\dagger)^N |\text{vac}\rangle$ and one finds $E(\mathbf{k}) \approx N$ at $\mathbf{k} = \hat{\mathbf{k}} := (\pi/a, \pi/a)$. We thus expect the entanglement to decrease when increasing the lattice depth.

Results – In Fig. 2 we show $E(\mathbf{k})$ in the first Brillouin zone for $s = 9, 12, 15, 18, 21$. For each value of s we collected ≈ 40 absorption images in order to reduce the statistical error on the determination of the entanglement. Relative shot-to-shot spread of the atom number is lower than 10%. The lower bound of the entanglement decreases as the system crosses the transition from the superfluid (lower s values) to the Mott insulator phase ($s > 15$). This behavior can be seen better in Fig. 3, reporting the value of $E(k_x, k_y)$ averaged over a box of 5×5 pixels around $\hat{\mathbf{k}}$, where we expect [9] and found the bound to be largest. Details of our imaging system are explained in Appendix D, where we also describe the error analysis.

As the entanglement of the system is expected to decrease with increasing temperature [9], we also perform measurements fixing the optical lattice depth s and varying the temperature of the atomic sample. The determination of the temperature inside the lattice is still challenging [42, 43] while its measurement in a harmonic potential, i.e., before raising the lattice, is routinely done. Here, we refer to the temperature T before the loading of the optical lattice. In practice, in order to

realize samples of different temperatures, we perform optical evaporation in the ODT to different values of the power P_{ODT} and then we increase the power of the optical dipole potential up to a fixed value P_1 . This procedure allowed us to obtain temperatures from 40 nK up to 100 nK in the same final harmonic potential before loading the lattices (see Appendix E for details). In Fig. 4 we show the behaviour of the minimal entanglement for different temperatures and for three different values of the lattice depth corresponding to a superfluid ground state ($s = 6$), a Mott insulator phase ($s = 18$), and the crossover region ($s = 12$). As expected [9], with increasing the temperature, the minimal entanglement consistent with the measurements decreases.

Conclusions & Outlook – We have quantified experimentally the multi-partite entanglement of a system of interacting bosons in an optical lattice through routinely done measurement of the atomic density profile after expansion. As the Hamiltonian and the ensuing dynamics of such a system can be controlled, it constitutes a bosonic *quantum simulator*, naturally supplying the resource entanglement at low temperatures. Our estimation of the entanglement is rigorous and without unspoken assumptions and provides a quantitative insight into the structure of the many-body state. In essence, we have answered the question, “Which is the least amount of entanglement that is consistent with given measurements?” [21]. The strategy we implemented for this estimation is sufficiently general to allow for its adaption and application in a wide variety of experimental settings that arise naturally in quantum science. Indeed, this principle may also be generalized to other quantities. One may for example ask what is the maximal entropy consistent with given measurement results and by answering this question place rigorous, assumption-free, upper bounds on the entropy of a quantum many-body systems. Of course, our approach is not restricted to bosonic systems but may also be applied to fermionic and spin systems or mixtures of bosonic and fermionic atoms, thus providing quantitative information about complex states of matter.

Acknowledgments

The work at Ulm University has been supported by the EU Integrated Project QESSENCE, the EU STREPs CORNER, the Alexander von Humboldt Professorship and the BMBF. The work at LENS has been supported by MIUR through PRIN nr. 2009TM7ERK_004, ERC Advanced Grant DISQUA, and IIT Seed Project ENCORE. The work of F.C. has been supported by EU FP7 Marie-Curie Programme (Intra-European Fellowship and Career Integration Grant) and by MIUR-FIRB grant (Project No. RBFR10M3SB). We thank Michele Modugno, Carlo Sias, Jianming Cai, and Gor Nikoghosyan for critical reading of the manuscript. F.C. acknowledges H. Wunderlich for fruitful discussions at the early stages of this project.

Author contributions

M.C., F.C. and M.B.P. proposed the project, M.C. and M.B.P. led the theory; A.B., N.F., L.F., C.F., S.R., and M.I. planned

and carried out the experiment with input from F.C. and M.C.; M.C. derived the monotone and analyzed the data with input from all other authors; All authors discussed the results; M.C.,

M.B.P. (F.C., N.F., C.F.) wrote the theory (experimental) part of the manuscript with input from all authors.

-
- [1] M.B. Plenio and S. Virmani, *Quant. Inf. Comp.* **7**, 1 (2007).
 [2] R. Horodecki, P. Horodecki, M. Horodecki and K. Horodecki, *Rev. Mod. Phys.* **81**, 865 (2009).
 [3] K. Audenaert, J. Eisert, M.B. Plenio, and R.F. Werner, *Phys. Rev. A* **66**, 042327 (2002).
 [4] M.B. Plenio, J. Eisert, J. Dreißig and M. Cramer, *Geometric entropy in harmonic lattice systems*, *Phys. Rev. Lett.* **94**, 060503 (2005).
 [5] J. Eisert, M. Cramer, and M.B. Plenio, *Rev. Mod. Phys.* **82**, 277 (2010).
 [6] T.J. Osborne and M.A. Nielsen, *Quant. Inf. Comp.* **1**, 45 (2002).
 [7] G. Vidal, *Phys. Rev. Lett.* **91**, 147902 (2003).
 [8] K. Vogel and H. Risken, *Phys. Rev. A* **40**, 2847 (1989).
 [9] M. Cramer, M.B. Plenio and H. Wunderlich, *Phys. Rev. Lett.* **106**, 020401 (2011).
 [10] P. Krammer, H. Kampermann, D. Bruss, R.A. Bertlmann, L.C. Kwek and C. Macchiavello, *Phys. Rev. Lett.* **103**, 100502 (2009).
 [11] D. Leibfried, E. Knill, S. Seidelin, J. Britton, R.B. Blakestad, J. Chiaverini, D.B. Hume, W.M. Itano, J.D. Jost, C. Langer, R. Ozeri, R. Reichle, and D.J. Wineland, *Nature* **438**, 639 (2005).
 [12] H. Häffner, W. Hänsel, C.F. Roos, J. Benhelm, D. Chek-al-kar, M. Chwalla, T. Körber, U.D. Rapol, M. Riebe, P.O. Schmidt, C. Becher, O. Gühne, W. Dür, and R. Blatt, *Nature* **438**, 643 (2005).
 [13] T. Monz, P. Schindler, J.T. Barreiro, M. Chwalla, D. Nigg, W.A. Coish, M. Harlander, W. Hänsel, M. Hennrich, and R. Blatt, *Phys. Rev. Lett.* **106**, 130506 (2011).
 [14] X.-C. Yao, T.-X. Wang, P. Xu, H. Lu, G.-S. Pan, X.-H. Bao, C.-Z. Peng, C.-Y. Lu, Y.-A. Chen, and J.-W. Pan, *Nat. Photonics* **6**, 225 (2012).
 [15] J. Estève, C. Gross, A. Weller, S. Giovanazzi, and M.K. Oberthaler, *Nature* **455**, 1216 (2008).
 [16] I.D. Leroux, M.H. Schleier-Smith, and V. Vuletić, *Phys. Rev. Lett.* **104**, 250801 (2010).
 [17] M.F. Riedel, P. Böhi, Y. Li, T.W. Hänsch, A. Sinatra, and P. Treutlein, *Nature* **464**, 1170 (2010).
 [18] A. Louchet-Chauvet, J. Appel, J. J. Renema, D. Oblak, N. Kjaergaard and E. S. Polzik, *New. Journal of Phys.* **12**, 065032 (2010).
 [19] O. Mandel, M. Greiner, A. Widera, T. Rom, T.W. Hänsch, and I. Bloch, *Nature* **425**, 937 (2003).
 [20] N.B. Christensen, H.M. Ronnow, D.F. McMorrow, A. Harrison, T.G. Perring, M. Enderle, R. Coldea, L.P. Regnault, and G. Aeppli, *Proc. Nat. Acad. Sci. USA* **104**, 15264 (2007).
 [21] K.M.R. Audenaert and M.B. Plenio, *New J. Phys.* **8**, 266 (2006).
 [22] J. Eisert, F.G.S.L. Brandão and K.M.R. Audenaert, *New J. Phys.* **9**, 46 (2007).
 [23] R. Horodecki, M. Horodecki and P. Horodecki, *Phys. Rev. A* **59**, 1799 (1999).
 [24] F.G.S.L. Brandão and M.B. Plenio, *Nat. Phys.* **4**, 873 - 877 (2008).
 [25] G. Gour and R.W. Spekkens, *New J. Phys.* **10**, 033023 (2008).
 [26] L.I. Masanes, *Phys. Rev. Lett.* **96**, 150501 (2006).
 [27] C.H. Bennett, G. Brassard, C. Crépeau, R. Jozsa, A. Peres and W.K. Wootters, *Phys. Rev. Lett.* **70**, 1895 (1993).
 [28] J. Eisert, K.A. Jacobs, P. Papadopoulos, and M.B. Plenio, *Phys. Rev. A* **62**, 052317 (2000).
 [29] H.M. Wiseman and J.A. Vaccaro, *Phys. Rev. Lett.* **91**, 097902 (2003).
 [30] F. Verstraete and J.I. Cirac, *Phys. Rev. Lett.* **91**, 010404 (2003).
 [31] N. Schuch, F. Verstraete, J.I. Cirac, *Phys. Rev. Lett.* **92**, 087904 (2004).
 [32] K.G.H. Vollbrecht and J.I. Cirac, *Phys. Rev. Lett.* **98**, 190502 (2007).
 [33] O. Gühne and G. Toth, *Phys. Rep.* **474**, 1 (2009).
 [34] F.G.S.L. Brandão, *Phys. Rev. A* **72**, 022310 (2005).
 [35] The estimated temperature of the condensate is < 50 nK corresponding to a condensate fraction bigger than 80%.
 [36] Y.J. Lin, A.R. Perry, R. L. Compton, I.B. Spielman, J.V. Porto, *Phys. Rev. A* **79**, 063631 (2009).
 [37] M. Endres, M. Cheneau, T. Fukuhara, C. Weitenberg, P. Schauss, C. Gross, L. Mazza, M. C. Banuls, L. Pollet, I. Bloch, and S. Kuhr, *Science* **334**, 200 (2011).
 [38] D. Jaksch, C. Bruder, J.I. Cirac, C.W. Gardiner, and P. Zoller, *Phys. Rev. Lett.* **81**, 3108 (1998).
 [39] M. Greiner, O. Mandel, T. Esslinger, T.W. Hänsch, and I. Bloch, *Nature* **415**, 39 (2002).
 [40] P. Pedri, L. Pitaevskii, S. Stringari, C. Fort, S. Burger, F.S. Cataliotti, P. Maddaloni, F. Minardi, and M. Inguscio, *Phys. Rev. Lett.* **87**, 220401 (2001).
 [41] F. Gerbier, S. Trotzky, S. Foelling, U. Schnorrberger, J.D. Thompson, A. Widera, I. Bloch, L. Pollet, M. Troyer, B. Capogrosso-Sansone, N.V. Prokofev, and B.V. Svistunov, *Phys. Rev. Lett.* **101**, 155303 (2008).
 [42] N. Gemelke, X. Zhang, C.-L. Hung, and C. Chin, *Nature* **460**, 995 (2009).
 [43] D. M. Weld, P. Medley, H. Miyake, D. Hucul, D. E. Pritchard, and W. Ketterle, *Phys. Rev. Lett.* **103**, 245301 (2009).
 [44] D. Steck, <http://steck.us/alkalidata>
 [45] G. Reinaudi, T. Lahaye, Z. Wang, D. Guéry-Odelin, *Opt. Lett.* **32**, 3143 (2007).

Appendix A: An illustrative example

We illustrate the resource character of states that are not of the form Eq. (1) by means of an example taken from Ref. [30]. Suppose a single classical bit is encoded in the relative phase of the two states

$$|\pm\rangle = \frac{1}{\sqrt{2}}(|0\rangle_A|1\rangle_B \pm |1\rangle_A|0\rangle_B). \quad (\text{A1})$$

Remarkably, if Alice and Bob are constrained by LOCC and local particle number conservation, they are unable to distinguish these two states – the bit \pm is hidden from them. They may learn the bit, however, in one of two different ways: (i) if

they share entanglement in the form

$$|\psi\rangle = \frac{1}{\sqrt{N+1}} \sum_{n=0}^N |n\rangle_A |N-n\rangle_B, \quad (\text{A2})$$

which has $\langle\psi|\hat{N}|\psi\rangle = N$, $\text{tr}_B[|\psi\rangle\langle\psi|]$ and $\text{tr}_A[|\psi\rangle\langle\psi|]$ commute with the respective local number operators, but it may *not* be written as in Eq. (1). Or (ii) if they share the state ($z = |\alpha|e^{i\phi}$)

$$\hat{\rho} \propto \int_0^{2\pi} d\phi |z\rangle_A \langle z| \otimes |z\rangle_B \langle z|, \quad |z\rangle \propto \sum_{n=0}^{\infty} \frac{z^n}{\sqrt{n!}} |n\rangle, \quad (\text{A3})$$

which is of the form in Eq. (1), commutes with the total number operator, and has $\langle\hat{N}\rangle = \text{tr}[\hat{N}\hat{\rho}] = 2|\alpha|^2$.

Now, the success probability of learning the phase of $|\pm\rangle$ increases with $\langle\hat{N}\rangle$ (approaching unity as $\langle\hat{N}\rangle \rightarrow \infty$), or, in other words, the value of these resource states increases as their mean total number of particles with $\langle\hat{N}\rangle$ increases. For $|\psi\rangle$ the entanglement increases while for $\hat{\rho}$ the local violation of particle number conservation increases.

Let us evaluate the lower bound in Eq. (5) for these states. Suppose that the lattice consists of the two sites $\mathbf{a} = \mathbf{0}$ and $\mathbf{b} = (1\ 0\ 0)^t$, which we associate with Alice and Bob, respectively. For the states in Eq. (A2) and Eq. (A3), we find

$$E(\mathbf{k} = (\pi/a)) = \begin{cases} \frac{2}{N+1} \sum_{n=0}^{N-1} \sqrt{n+1} \sqrt{N-n}, \\ 2|\alpha|^2 = \text{tr}[\hat{N}\hat{\rho}], \end{cases} \quad (\text{A4})$$

respectively. Hence, for both states, we have a lower bound to the entanglement that is increasing in $\langle\hat{N}\rangle$ (thus capturing the value of these states for the above data-hiding protocol) and for the second state the bound is in fact exact as $\mathcal{E}(\hat{\rho}) \leq \text{tr}[\hat{N}\hat{\rho}]$ for all states $\hat{\rho}$.

Appendix B: A monotone under SSR-LOCC operations

Here we show that

$$\mathcal{E}(\hat{\rho}) = \max\left\{0, -\inf_{\hat{W} \in \mathcal{W}} \text{tr}[\hat{W}\hat{\rho}]\right\} \quad (\text{B1})$$

is a monotone under LOCC operations commuting with the local particle number operators. Let the Hilbert space \mathcal{H} be a direct product of \mathcal{G} parties, $\mathcal{H} = \bigotimes_{s=1}^{\mathcal{G}} \mathcal{H}_s$. LOCC operations with respect to this partition are operations taking density matrices $\hat{\rho}$ to $\sum_k p_k \hat{\rho}_k$, where $\hat{\rho}_k = \hat{A}_k \hat{\rho} \hat{A}_k^\dagger / p_k$, $p_k = \text{tr}[\hat{A}_k \hat{\rho} \hat{A}_k^\dagger]$ and the \hat{A}_k are of the form $\hat{A}_k = \bigotimes_{s=1}^{\mathcal{G}} \hat{A}_s^k$ and fulfil $\sum_k \hat{A}_s^k \hat{A}_s^k \leq \mathbb{1}$ and $[\hat{A}_s^k, \hat{n}_s] = 0$. $\mathcal{E}(\hat{\rho})$ is an entanglement monotone if

$$\sum_k p_k E(\hat{\rho}_k) \leq \mathcal{E}(\hat{\rho}). \quad (\text{B2})$$

For all $\hat{W} \in \mathcal{W}$, we have $\text{tr}[\hat{W}\hat{\rho}_k] \geq -\text{tr}[\hat{N}\hat{\rho}_k] > -\infty$. Hence, the infimum exists and we denote it by E_k . Now let

$\epsilon > 0$. Then $E_k + \epsilon$ is not an infimum and therefore there is an $\hat{W}_{k,\epsilon} \in \mathcal{W}$ such that $\text{tr}[\hat{W}_{k,\epsilon}\hat{\rho}_k] < E_k + \epsilon$, i.e.,

$$\begin{aligned} \sum_k p_k E(\hat{\rho}_k) &= -\sum_{\substack{k \\ E_k < 0}} p_k E_k < \sum_{\substack{k \\ E_k < 0}} p_k (\epsilon - \text{tr}[\hat{W}_{k,\epsilon}\hat{\rho}_k]) \\ &\leq \epsilon - \text{tr}\left[\left(\sum_{k: E_k < 0} \hat{A}_k^\dagger \hat{W}_{k,\epsilon} \hat{A}_k\right)\hat{\rho}\right], \end{aligned} \quad (\text{B3})$$

which is upper bounded by

$$\sum_k p_k E(\hat{\rho}_k) \leq \epsilon - \inf_{\hat{W} \in \mathcal{W}} \text{tr}[\hat{W}\hat{\rho}], \quad (\text{B4})$$

as the operator in brackets in Eq. (B3) is a member of \mathcal{W} : For all k and all ϵ , we have $\hat{W}_{k,\epsilon} + \hat{N} \geq 0$, i.e.,

$$0 \leq \sum_{\substack{k \\ E_k < 0}} \hat{A}_k^\dagger (\hat{W}_{k,\epsilon} + \hat{N}) \hat{A}_k \leq \sum_{\substack{k \\ E_k < 0}} \hat{A}_k^\dagger \hat{W}_{k,\epsilon} \hat{A}_k + \hat{N} \quad (\text{B5})$$

as $[\hat{A}_k, \hat{N}] = 0$ for all k . Now let $\hat{\sigma} \in \mathcal{S}$. Then

$$\text{tr}\left[\left(\sum_{\substack{k \\ E_k < 0}} \hat{A}_k^\dagger \hat{W}_{k,\epsilon} \hat{A}_k\right)\hat{\sigma}\right] = \sum_{\substack{k \\ E_k < 0}} \text{tr}[\hat{W}_{k,\epsilon} \hat{A}_k \hat{\sigma} \hat{A}_k^\dagger], \quad (\text{B6})$$

where, up to normalization, $\hat{A}_k \hat{\sigma} \hat{A}_k^\dagger \in \mathcal{S}$, i.e., the above is lower bounded by zero (as $\hat{W}_{k,\epsilon} \in \mathcal{W}$) and we hence have that for all $\epsilon > 0$

$$\sum_k p_k E(\hat{\rho}_k) < \epsilon - \inf_{\hat{W} \in \mathcal{W}} \text{tr}[\hat{W}\hat{\rho}] \leq \epsilon + E(\hat{\rho}), \quad (\text{B7})$$

which implies that \mathcal{E} is an entanglement monotone.

Appendix C: Density after time-of-flight

We set out to derive an expression of the atomic column density after free evolution, i.e., after evolution under the Hamiltonian

$$\hat{H} = \int d\mathbf{r} \hat{\Psi}^\dagger(\mathbf{r}) \left[-\frac{\hbar^2}{2m} \nabla^2 \right] \hat{\Psi}(\mathbf{r}). \quad (\text{C1})$$

In order to connect the atomic column density to observables in the lattice, i.e., before the free expansion, we expand the field operators in Wannier functions of the lattice

$$\hat{\Psi}(\mathbf{r}) = \sum_{\mathbf{i}} w_{\mathbf{i}}(\mathbf{r}) \hat{b}_{\mathbf{i}}. \quad (\text{C2})$$

Here \mathbf{i} is a multi-index containing the lattice site and the band index. The density operator after evolution under \hat{H} for a time t reads

$$\begin{aligned} \hat{n}(\mathbf{r}, t) &:= e^{it\hat{H}/\hbar} \hat{\Psi}^\dagger(\mathbf{r}) \hat{\Psi}(\mathbf{r}) e^{-it\hat{H}/\hbar} \\ &= \sum_{\mathbf{i}, \mathbf{j}} w_{\mathbf{i}}^*(\mathbf{r}) w_{\mathbf{j}}(\mathbf{r}) e^{it\hat{H}/\hbar} \hat{b}_{\mathbf{i}}^\dagger \hat{b}_{\mathbf{j}} e^{-it\hat{H}/\hbar}. \end{aligned} \quad (\text{C3})$$

Now, due to the lattice geometry, the Wannier functions factorize and are the same for each spatial direction, $w_i(\mathbf{r}) = w_{i_x}(x)w_{i_y}(y)w_{i_z}(z)$. Owing to orthonormality, we hence find for the column-density operator $\hat{n}(x, y, t) := \int dz \hat{n}(\mathbf{r}, t)$ after time-of-flight t

$$\hat{n}(x, y, t) = \sum_{\substack{\mathbf{i}, \mathbf{j} \\ i_z = j_z}} w_{i_x}^*(x)w_{j_x}(x)w_{i_y}^*(y)w_{j_y}(y)\hat{b}_{\mathbf{i}}^\dagger(t)\hat{b}_{\mathbf{j}}(t).$$

To compute the time-evolution $\hat{b}_{\mathbf{i}}(t) = e^{it\hat{H}/\hbar}\hat{b}_{\mathbf{i}}e^{-it\hat{H}/\hbar}$ of the bosonic annihilation operators, we expand in orthonormal and complete plane waves $\omega(\mathbf{r}) = e^{2\pi i \mathbf{p} \cdot \mathbf{r}/L}/L^{3/2}$,

$$\hat{\Psi}(\mathbf{r}) = \sum_{\mathbf{p}} \omega_{\mathbf{p}}(\mathbf{r})\hat{a}_{\mathbf{p}}. \quad (\text{C4})$$

Due to orthonormality, the bosonic annihilation operators are related as

$$\hat{b}_{\mathbf{i}} = \sum_{\mathbf{p}} \langle w_{\mathbf{i}}, \omega_{\mathbf{p}} \rangle \hat{a}_{\mathbf{p}}, \quad \hat{a}_{\mathbf{p}} = \sum_{\mathbf{i}} \langle \omega_{\mathbf{p}}, w_{\mathbf{i}} \rangle \hat{b}_{\mathbf{i}}, \quad (\text{C5})$$

where we denoted $\langle f, g \rangle = \int d\mathbf{r} f^*(\mathbf{r})g(\mathbf{r})$. The Hamiltonian is diagonal in the basis of the $\hat{a}_{\mathbf{p}}$,

$$\hat{H} = \frac{2\pi^2 \hbar^2}{L^2 m} \sum_{\mathbf{p}} \mathbf{p}^2 \hat{a}_{\mathbf{p}}^\dagger \hat{a}_{\mathbf{p}}, \quad (\text{C6})$$

which implies

$$e^{it\hat{H}/\hbar} \hat{a}_{\mathbf{p}} e^{-it\hat{H}/\hbar} = e^{-it \frac{2\pi^2 \hbar}{L^2 m} \mathbf{p}^2} \hat{a}_{\mathbf{p}}, \quad (\text{C7})$$

i.e., using Eqs. (C5),

$$\hat{b}_{\mathbf{i}}(t) = \sum_{\mathbf{p}} \sum_{\mathbf{j}} \langle w_{\mathbf{i}}, \omega_{\mathbf{p}} \rangle \langle \omega_{\mathbf{p}}, w_{\mathbf{j}} \rangle e^{-it \frac{2\pi^2 \hbar}{L^2 m} \mathbf{p}^2} \hat{b}_{\mathbf{j}}.$$

Hence,

$$\hat{n}(x, y, t) = \sum_{\substack{\mathbf{p}, \mathbf{q}, \mathbf{i}, \mathbf{j} \\ i_z = j_z}} w_{i_x}^*(x)w_{j_x}(x)w_{i_y}^*(y)w_{j_y}(y) \langle \omega_{\mathbf{p}}, w_{\mathbf{i}} \rangle \langle w_{\mathbf{j}}, \omega_{\mathbf{q}} \rangle e^{it \frac{2\pi^2 \hbar}{L^2 m} (\mathbf{p}^2 - \mathbf{q}^2)} \hat{a}_{\mathbf{p}}^\dagger \hat{a}_{\mathbf{q}}, \quad (\text{C8})$$

where completeness and orthonormality imply $\sum_{i_z} \langle \omega_{p_z}, w_{i_z} \rangle \langle w_{i_z}, \omega_{q_z} \rangle = \delta_{p_z, q_z}$ and $\sum_j w_j(x) \langle w_j, \omega_q \rangle = \omega_q(x)$, i.e.,

$$\hat{n}(x, y, t) = \sum_{\substack{\mathbf{p}, \mathbf{q} \\ p_z = q_z}} \omega_{p_x}^*(x)\omega_{q_x}(x)\omega_{p_y}^*(y)\omega_{q_y}(y) e^{it \frac{2\pi^2 \hbar}{L^2 m} (\mathbf{p}^2 - \mathbf{q}^2)} \hat{a}_{\mathbf{p}}^\dagger \hat{a}_{\mathbf{q}}. \quad (\text{C9})$$

Now, again using Eqs. (C5), we arrive at an expression for the column density in terms of the $\hat{b}_{\mathbf{i}}$

$$\hat{n}(x, y, t) = \sum_{\substack{\mathbf{i}, \mathbf{j} \\ i_z = j_z}} g_{\mathbf{i}}^*(\mathbf{r}, t) g_{\mathbf{j}}(\mathbf{r}, t) \hat{b}_{\mathbf{i}}^\dagger \hat{b}_{\mathbf{j}}, \quad (\text{C10})$$

where $g_{\mathbf{i}}(\mathbf{r}, t) = g_{i_x}(x, t)g_{i_y}(y, t)$, with

$$\begin{aligned} g_{\mathbf{i}}(x, t) &= \sum_q \omega_q(x) \langle \omega_q, w_{\mathbf{i}} \rangle e^{-it \frac{2\pi^2 \hbar}{L^2 m} q^2} \\ &= \frac{1}{\sqrt{L}} \sum_q e^{2\pi i q x / L} \langle \omega_q, w_{\mathbf{i}} \rangle e^{-it \frac{2\pi^2 \hbar}{L^2 m} q^2}, \end{aligned} \quad (\text{C11})$$

and we used completeness and orthonormality to arrive at $\sum_{p_z} \langle w_{i_z}, \omega_{p_z} \rangle \langle \omega_{p_z}, w_{j_z} \rangle = \delta_{i_z, j_z}$. Finally, considering the properties of the Wannier functions, and after some algebra, we let $L \rightarrow \infty$ to obtain

$$\begin{aligned} \frac{g_{\mathbf{i}}(x, t)}{\sqrt{2\pi}} &= e^{i \frac{\pi^2}{\tau} (x/a - i)^2} \int_{-\infty}^{\infty} d\phi e^{-i\tau \phi^2} \bar{w}_n(\phi + \frac{\pi}{a\tau} x - \frac{\pi}{\tau} i) \\ &=: e^{i \frac{\pi^2}{\tau} (x/a - i)^2} \frac{f_{\mathbf{i}}(x)}{\sqrt{2\pi}}, \end{aligned}$$

where $\tau = t \frac{2\pi^2 \hbar}{ma^2}$ and

$$\bar{w}_n(\phi) = \frac{1}{\sqrt{2\pi}} \int_{-\infty}^{\infty} dr w_{0,n}(ar) e^{-2\pi i \phi r} \quad (\text{C12})$$

is the Fourier transform of the Wannier function of the n 'th band centred at zero. Eq. (C10) with $g_{\mathbf{i}}$ as above is the exact expression for the column density at (x, y) . All the involved functions may be obtained by a numerical calculation of the Wannier functions.

In the experiment, only the lowest band is occupied and we omit the band index from now on. In the stationary phase approximation, which is valid for $1 \ll \tau$ ($\approx 1.8 \times 10^3$ in our experiment), one has

$$f_{\mathbf{i}}(x) \approx (1 - i) \frac{\pi}{\sqrt{\tau}} \bar{w}(\frac{\pi}{a\tau} x - \frac{\pi}{\tau} i). \quad (\text{C13})$$

Finally, approximating $\bar{w}(\frac{\pi}{a\tau} x - \frac{\pi}{\tau} i) \approx \bar{w}(\frac{\pi}{a\tau} x)$ [41], yields

$$\hat{n}(\mathbf{r} = \frac{\hbar t}{m} \mathbf{k}, t) = f(\mathbf{k}) \sum_{\substack{\mathbf{i}, \mathbf{j} \\ i_z = j_z}} e^{i[a\mathbf{k}(\mathbf{i} - \mathbf{j}) + \pi^2(\mathbf{j}^2 - \mathbf{i}^2)/\tau]} \hat{b}_{\mathbf{i}}^\dagger \hat{b}_{\mathbf{j}},$$

for the column density at $\mathbf{r} = (x, y) = \hbar t(k_x, k_y)/m = \hbar t \mathbf{k}/m = \tau a^2 \mathbf{k}/(2\pi^2)$ after a time-of-flight t . Here,

$$f(\mathbf{k}) = \frac{m^2 a^4}{\hbar^2 t^2} |w(\frac{a}{2\pi} k_x)|^2 |w(\frac{a}{2\pi} k_y)|^2, \quad (C14)$$

$$w(\frac{a}{2\pi} k) = \frac{1}{\sqrt{2\pi}} \int_{-\infty}^{\infty} dr w_0(ar) e^{-ikar},$$

and w_0 is the Wannier function of the lowest band centred at zero.

Appendix D: Image and error analysis

We intend now to analyze the measurement of

$$E(x, y) = \langle \hat{N} \rangle - \frac{\langle \hat{n}(x, y) \rangle}{f(x, y)}, \quad (D1)$$

where we now work in real-space coordinates, i.e., $\langle \hat{n}(x, y) \rangle = \int dz \langle \hat{n}(x, y, z) \rangle$, where $\langle \hat{n}(x, y, z) \rangle$ is the expectation value of the density distribution of the atom cloud at $\mathbf{r} = (x, y, z)$ after time-of-flight and

$$f(x, y) = \frac{m^2 a^4}{\hbar^2 t^2} |w(\frac{am}{2\pi \hbar t} x)|^2 |w(\frac{am}{2\pi \hbar t} y)|^2 \quad (D2)$$

as in Eq. (C14).

Due to the spatial discretization of the CCD sensor used in the experiment, we define the discrete function

$$E'_{i,j} := \frac{1}{\Delta^2} \int_{\Delta_i} dx \int_{\Delta_j} dy E(x, y) \quad (D3)$$

$$= \langle \hat{N} \rangle - \frac{1}{\Delta^2} \int_{\Delta_i} dx \int_{\Delta_j} dy \frac{\langle \hat{n}(x, y) \rangle}{f(x, y)}$$

where (i, j) denotes the index of each pixel, centered on (x_i, y_j) , and $\Delta_{i,j} = [x_{i,j} - \Delta/2, x_{i,j} + \Delta/2]$. $\Delta = 2.78 \mu\text{m}$ is the effective pixel size which takes into account the physical pixel size and the magnification of the imaging system. The total number of atom is given by $N = \sum_{i,j} n_{i,j}$. Note that the quantity $E'_{i,j}$ is still a lower bound for all (i, j) .

For each acquired image, we incorporate the symmetry of the observable $\hat{n}(\mathbf{k})/f(\mathbf{k})$ by averaging over pixels corresponding to (k_x, k_y) , $(k_x \pm 2\pi/a, k_y \pm 2\pi/a)$, and the symmetry of the experimental setup by averaging also over the four points $(\pm k_x, \pm k_y)$. For Figs. 3 and 4, we additionally consider the average of $E'_{i,j}$ on a subset of 5×5 pixels (corresponding to twice the width of the point spread function of the imaging system) centered around $\mathbf{k} \in [-2\pi/a, 2\pi/a]^{\times 2}$, where a is the lattice spacing. If we define a set of pixels A over which we perform the average, the quantity

$$E'_A := \frac{1}{|A|} \sum_{(i,j) \in A} E'_{i,j}, \quad (D4)$$

is also a lower bound to the entanglement.

Actually, we do not have access to the quantity $n(x, y)/f(x, y)$ to be integrated in Eq. (D3). Approximating (and taking the error into account below) the continuous

function f by $f(x, y) \approx f(x_i, y_j)$ for each $(x, y) \in (\Delta_i, \Delta_j)$, we introduce the simplified quantities E_A and $E_{i,j}$

$$E'_A \approx E_A := \frac{1}{|A|} \sum_{(i,j) \in A} \left(\langle \hat{N} \rangle - \frac{1}{\Delta^2} g_{i,j} \langle \hat{n}_{i,j} \rangle \right) \quad (D5)$$

$$=: \frac{1}{|A|} \sum_{(i,j) \in A} E_{i,j},$$

where $g_{i,j} = 1/f(x_i, y_j)$ and $\langle \hat{n}_{i,j} \rangle$ is the expected number of atoms recorded by pixel (i, j) .

In the experiment, we use a running average of about 40 density profiles for each value of lattice depth s and temperature T . The empirical average of E_A over a set of M images is also the best estimation of the entanglement bound E'_A

$$\bar{E}_A = \frac{1}{M} \sum_{n=1}^M E_A^{(n)} = \frac{1}{|A|} \sum_{(i,j) \in A} \bar{E}_{i,j}, \quad (D6)$$

$n = 1, \dots, M$ being the image index. We proceed by analyzing the sources of uncertainty when estimating E'_A , i.e., the systematic uncertainty related to $n_{i,j}$ and $g_{i,j}$, and the statistical contribution associated to shot-to-shot variations of $n_{i,j}$. The statistical uncertainty can be estimated as

$$(\sigma_{\bar{E}_A}^{stat})^2 = \frac{1}{M(M-1)} \sum_{n=1}^M \left(E_A^{(n)} - \bar{E}_A \right)^2. \quad (D7)$$

The approximation $g(x, y) \simeq g_{i,j}$ used in Eq. (D5) for $x \in \Delta_i, y \in \Delta_j$ introduces a systematic error. We find

$$|E'_{i,j} - E_{i,j}| \leq \int_{\Delta_i} dx \int_{\Delta_j} dy \frac{\langle \hat{n}(x, y) \rangle}{\Delta^2} |g(x, y) - g_{i,j}|. \quad (D8)$$

From the mean value theorem we have that

$$g_{i,j} - g(x, y) = (\partial_x g)(a, b)(x_i - x) + (\partial_y g)(a, b)(y_i - y),$$

where $(a, b) = (1-c)(x, y) + c(x_i, y_i)$ for some c between 0 and 1. Hence, for $x \in \Delta_i, y \in \Delta_j$, we find

$$|g_{i,j} - g(x, y)| \leq \frac{\Delta}{\sqrt{2}} \max_{a \in \Delta_i, b \in \Delta_j} |\nabla g(a, b)| =: \frac{\Delta}{\sqrt{2}} \epsilon_{i,j},$$

and with this result (D8) becomes

$$|E'_{i,j} - E_{i,j}| \leq \frac{1}{\sqrt{2}\Delta} \epsilon_{i,j} \langle \hat{n}_{i,j} \rangle. \quad (D9)$$

Thus, assuming a flat error distribution, the resulting standard error is given by

$$\sigma_{i,j} = \frac{1}{\sqrt{6}\Delta} \epsilon_{i,j} \langle \hat{n}_{i,j} \rangle. \quad (D10)$$

Now we analyze in more detail the other systematic contributions. In the following, we write $\mathbf{i} = (i, j)$. The g_i are obtained from the Wannier function of the optical lattice and

thus the error depends on the uncertainty $\sigma_s = 0.1s$ we have in the estimation of the lattice depth s , i.e.,

$$\sigma_{g_i}^2 = \sigma_s^2 (\partial_s g_i)^2. \quad (D11)$$

Now we discuss the systematic error on $n_i^{(n)}$. In the experiment, we measure the optical density distribution by absorption imaging. More specifically, we record on a CCD camera the intensity profile of a resonant probe laser beam interacting with the sample. The absorbed light intensity I_a , integrated along the z direction (the direction of propagation of the probe beam), as given by the Beer-Lambert law, is $I_a = I_0 \left(1 - \exp[-\sigma \int \hat{n}(\mathbf{r}) dz]\right)$, with I_0 being the incident intensity and σ the resonant absorption cross section given by $\sigma = 3\lambda_0^2/(2\pi)$, where λ_0 is the wavelength of the resonant transition. For circularly-polarized light on the transition we used for ^{87}Rb , we have $\sigma = 2.907 \cdot 10^{-13} \text{ m}^2$ [44]. Hence, one has

$$n_i = -\frac{1}{\sigma} \left(\frac{I_t - I_d}{I_0 - I_d} \right), \quad (D12)$$

where $I_t = I_0 - I_a$ is the transmitted light intensity, and I_d is the intensity of the background light recorded on the CCD camera without the imaging beam. Polarization effects and the atomic manifold level-structure of the optical transition used in the imaging process can bring the absorption cross-section to be smaller than its theoretical value given above. This would lead to underestimate the number of atoms. Thus, we perform an accurate calibration of the absorption imaging efficiency [45]. For the pixel i centered at (x_i, y_i) as denoted above, the atomic density is given by

$$n_i^{(n)} = \alpha (\mu_i^{(n)} - \mu_0^{(n)}), \quad (D13)$$

where the prefactor α and its uncertainty σ_α are given by

$$\alpha = 0.112, \quad \sigma_\alpha = 0.009, \quad (D14)$$

and $\mu_0^{(n)}$ is an offset that may vary from image to image (hence the index n). We estimate $\mu_0^{(n)}$ as follows. For pixels i far away from the centre of the image, we do not expect any atoms. We consider quadratic frames centred on the image of thickness one pixel and increasing size. We then calculate the average of $\mu_i^{(n)}$ for each frame and take $\mu_0^{(n)}$ as the minimum over all such frames and (F denotes the set of pixels corresponding to the frame)

$$\sigma_{\mu^{(n)}}^2 = \frac{1}{|F|} \sum_{i \in F} (\mu_i^{(n)} - \mu_0^{(n)})^2. \quad (D15)$$

To summarize, the best estimation of the entanglement bound over a set of M images is given by

$$\bar{E}_A = \frac{\alpha}{M} \sum_{n=1}^M \sum_i (\mu_i^{(n)} - \mu_0^{(n)}) \left(1 - \frac{g_i}{\Delta^2 |A|} \delta_{i \in A} \right),$$

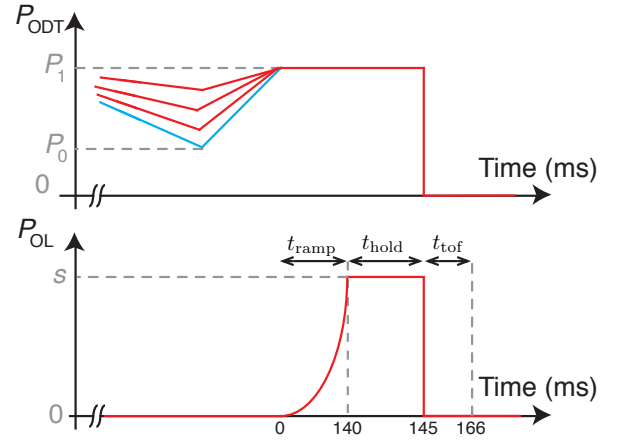


FIG. 5: Experimental sequence to obtain samples with different temperatures in the same final potential before ramping the lattices: Ramps of the optical dipole trap (ODT) and the optical lattice (OL). The value of P_0 corresponds to the power of the ODT at the end of the evaporation. It is tuned in order to realize samples of different temperatures.

and our best estimation of the systematic uncertainty is

$$(\sigma_{\bar{E}_A}^{sys})^2 = \sigma_\alpha^2 (\partial_\alpha \bar{E}_A)^2 + \sum_{n=1}^M \sigma_{\mu_0^{(n)}}^2 (\partial_{\mu_0^{(n)}} \bar{E}_A)^2 + \sum_{i \in A} \sigma_{g_i}^2 (\partial_{g_i} \bar{E}_A)^2, \quad (D16)$$

which evaluates to

$$(\sigma_{\bar{E}_A}^{sys})^2 = \frac{\sigma_\alpha^2 \bar{E}_A^2}{\alpha^2} + \frac{\alpha^2}{M^2} \left(\sum_{i \in A} \frac{g_i}{\Delta^2 |A|} - \sum_i 1 \right)^2 \sum_{n=1}^M \sigma_{\mu_0^{(n)}}^2 + \frac{1}{\Delta^4 |A|^2} \sum_{i \in A} \sigma_{g_i}^2 \bar{n}_i^2.$$

The global uncertainty can be found adding systematic and statistical errors in quadrature,

$$\sigma_{E'_A}^2 = (\sigma_{\bar{E}_A}^{sys})^2 + (\sigma_{\bar{E}_A}^{stat})^2 + \frac{1}{|A|^2} \sum_{(i,j) \in A} \sigma_{i,j}^2, \quad (D17)$$

which corresponds to the error bars indicated in the main text. Analyzing the different contributions, we have found that the main error sources are related to the estimation of α and $\mu_0^{(n)}$, hence the error bars actually do not decrease when considering a larger number of images, i.e. statistical errors are negligible. In other words, our entanglement estimation does not require a large set of absorption images in order to get small errors on the lower bound.

Appendix E: Production of samples with different temperatures

In Fig. 5 we show the experimental sequence adopted to obtain samples with different temperature T (the temperature

before ramping up the lattice) in the same harmonic potential. As the temperature is varied through a final evaporation performed lowering the power P_{ODT} of the optical dipole trap to a final value P_0 , in general samples with different temperatures are obtained in different harmonic potentials. For this reason, before ramping up the lattices we adiabatically increase in 500 ms the ODT to a fixed power P_1 . In this way all the

samples with different temperatures are prepared in the same harmonic potential with cylindrical symmetry characterized by a radial frequency of 50 Hz and an axial frequency of 8 Hz. The atom number in the samples with different temperatures is kept constant by varying the loading time of the magnetic trap in order to realize samples with similar atom number.